

Experience with four-component iterative Gabor deconvolution

David C. Henley and Gary F. Margrave

ABSTRACT

The seismic processing operation of deconvolution is aimed at removing as many of the earth's filtering effects on a set of seismic data as possible. The Gabor algorithm was first incorporated into deconvolution to accommodate the known non-stationarity of seismic data. Subsequent improvements enabled it to accommodate localized surface-related effects, as well as the more slowly varying Q effects. An algorithm recently developed for ProMAX derives, in the Gabor magnitude spectral domain, individual deconvolution operators which consist of four components; two attributable to source and receiver surface locations, one to midpoint location, and one to source-receiver offset. Because the initial factorized estimates of these components are somewhat ad hoc, the latest version of the algorithm allows iterative improvements of the components using a scheme resembling the ART algorithm used in transmission tomography and other applications. We show here results of using the new algorithm, compared to the older *Gabor2* algorithm, which was capable of only single trace deconvolution or ensemble average deconvolution. All results are real data. In general, we find the four-component algorithm provides broader bandwidth than the ensemble average Gabor operation and better event phase stability than the single-trace Gabor algorithm. Also, no more than two iterations appear to be necessary to reach a stable result in the *Gabor_sc* algorithm.

INTRODUCTION

The ideal seismic image for an interpreter shows sharply resolved reflection boundaries, with uniform spectral bandwidth throughout and no amplitude variations that are unrelated to actual rock property changes. The earliest deconvolution algorithms sought only to sharpen the resolution of individual traces with a single operator, making various assumptions regarding the shape of the underlying earth spectrum, and of the outgoing source wavelet. Later efforts attempted to account for effects of the earth's near-surface in the vicinity of a shot or receiver by deriving operators averaged over a source or receiver ensemble, thus becoming 'surface-consistent'. Still other efforts attempted to estimate the earth's intrinsic frequency-dependent attenuation in order to compensate the traces for Q and provide a spectrum more consistent over depth. Recently, the Gabor Transform was introduced by Margrave et al (2001, 2002) as a basis for analysis and derivation of non-stationary deconvolution operators. In its initial versions, Gabor deconvolution delivered impressive results with a more 'geological' look than some other rival processes because of its lack of a priori constraints on spectra (other than the very general assumption that a 'wavelet' spectrum should be 'smoother' than the 'earth' spectrum). In most comparisons, results from the Gabor deconvolution algorithm operating in single trace mode were at least as broad in bandwidth as results from more conventional algorithms.

One shortcoming of the Gabor single trace algorithm, highlighted by a study initiated by Mike Perz et al (2005), was that under certain extreme conditions involving groups of input traces with widely varying levels of additive random noise, the apparent phase of

some events could vary from trace to trace, depending upon the noise level of the input trace. As well, the original Gabor algorithm could not respond properly to input gathers which stand out in some way from their neighbors (having higher noise, lower signal, noise bursts, etc). In each case, the single-trace algorithm attempts to provide the widest bandwidth results possible from each trace, regardless of results from neighboring traces. While this is not necessarily incorrect, it means that images composed of blends of traces with widely varying bandwidths will be inconsistent, especially when the minimum phase constraint is applied in the deconvolution.

While some of these concerns could be addressed by simply using the original Gabor algorithm in ensemble average mode, at least three passes of the algorithm would be required (shot, receiver, and midpoint gathers), with only partial whitening at each stage. Hence, Montana and Margrave (2006) created a version of Gabor deconvolution which constructed operators from components averaged over shot, receiver, and midpoint, the so-called surface-consistent Gabor algorithm. Based on the success of this algorithm, a version was written for ProMAX which includes a fourth component, averaged over source-receiver offset (to accommodate systematic AVO effects) Henley et al (2007). An additional feature which was incorporated into this algorithm was the ability to re-estimate and improve each of the four components with additional passes through the raw data. The rationale for this is the rather ad hoc ‘factorization’ applied to the Gabor magnitude transform of each input trace to give the initial estimates of the four components. While the factorization seems to give pretty good results on most data, one or two iterations seem to improve the results on at least some data (probably dependent upon the noise content and variability of the input data).

The present work shows comparisons of results from the new algorithm (*Gabor_sc*) for the first estimate and two iterations compared to earlier results with the *Gabor2* algorithm in both ensemble average mode and single trace mode.

ALGORITHM DETAILS

Below is a step-by-step description of the ProMAX algorithm, *Gabor_sc*, which applies the four-component iterative version of Gabor deconvolution.

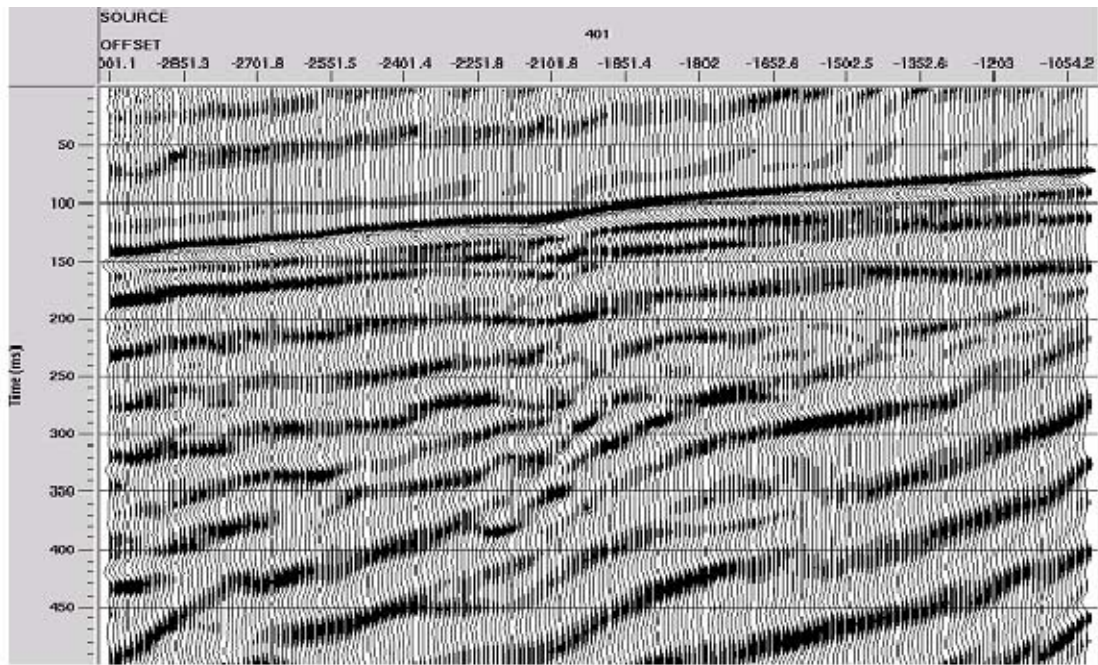
- Read a raw seismic trace, perform the Gabor Transform to obtain the Gabor magnitude spectrum, $|G|$.
- Apply hyperbolic smoothing (e.g. Margrave et al., 2004) to $|G|$ to derive a Q-function, $Qf = h(|G|)$, where $h(\cdot)$ indicates the hyperbolic smoothing operation, and to separate out the smoothed residual Gabor magnitude spectrum, $s(|G|/Qf)$, where $s(\cdot)$ indicates another (not hyperbolic) smoothing operation.

- Factor the Q-function (square root) and sum the result, \sqrt{Qf} , to deconvolution operator arrays indexed by source-receiver offset, D_o , and by midpoint (CDP), D_m .
- Factor the smoothed residual Gabor spectrum (square root) and sum the result, $\sqrt{s(G/Qf)}$, to deconvolution arrays indexed by source, D_s , and receiver, D_r .
- Repeat these steps until the entire data set has been read. Begin to read raw data again
- Read a raw seismic trace, perform the Gabor Transform to calculate anew the Gabor spectrum of the trace, G .
- Apply hyperbolic smoothing to re-estimate $Qf = h(|G|)$ and $s(|G|/Qf)$.
- Divide product of Q-function and residual magnitude spectrum by normalized products of three at a time of the four components estimated during the first pass. This provides new (iterated) estimates of each of the components in turn. For example, the updated source operator is $D'_s = s(|G|/Qf)Qf / (D_r D_o D_m)$ and similarly for the other components. These new estimates are summed into arrays indexed by source, receiver, offset, and midpoint.
- Retrieve the four component estimates from the first pass, whose source, receiver, offset, and midpoint correspond to those of the current trace, and combine into the magnitude of a deconvolution operator $|D| = D_s D_r D_m D_o$. Estimate the phase of the deconvolution operator by the usual Hilbert transform formula $\phi_D = H(\ln(|D|))$, where the Hilbert transform, H , is applied over frequency at constant time and the usual precautions are taken to avoid the log of zero. Apply the inverse Gabor transform to provide an output trace. At this time, we have assumed that all four components are minimum phase; however, this assumption could be modified by making any selected component zero phase for example.
- Repeat these steps until the data set has been read a second time.
- Modify initial component estimates by averaging with iterated estimates.
- Repeat for as many iterations as desired. Each iteration deconvolves the raw data with a revised operator.

TESTING TWO NEW DATA SETS

In order to illustrate the operation of the four-component Gabor algorithm, we apply it here to two different sets of field data; a small, very high resolution experimental 2D-3C data set from our Priddis field test site, and a larger 2D-3C data set of more conventional scale from the Spring Coulee survey, both acquired early in 2008. In 2007 (Henley et al), we compared an earlier version of the algorithm on Mike Perz' model data set as well as on the well-known Blackfoot 2D-3C data set. Both tests confirmed our intuitive prediction of how the algorithm would behave, compared to the earlier version of Gabor deconvolution, *Gabor2*. What we found in our experience with the earlier algorithm was that the four-component *Gabor_sc* seemed to combine the characteristics of the single-trace mode of *Gabor2* and the ensemble mode of the same algorithm, and that iterative estimation of the deconvolution operator factors seemed to provide some improvement of the overall results, although the effect is often quite subtle. Also noted was the tendency of the earlier algorithm to be unstable in its iterative estimations after more than two iterations and to begin to produce deconvolved results alternately dominated by high and low frequencies. Early in 2008, we modified the algorithm's SIRT-like iteration scheme so that new component estimates are always averaged with the current values before updating the component. This damping action appears to ensure that the present algorithm always approaches a stable solution. When tested on several different data sets with up to eight iterations, incremental differences in deconvolved results became insignificant after two iterations.

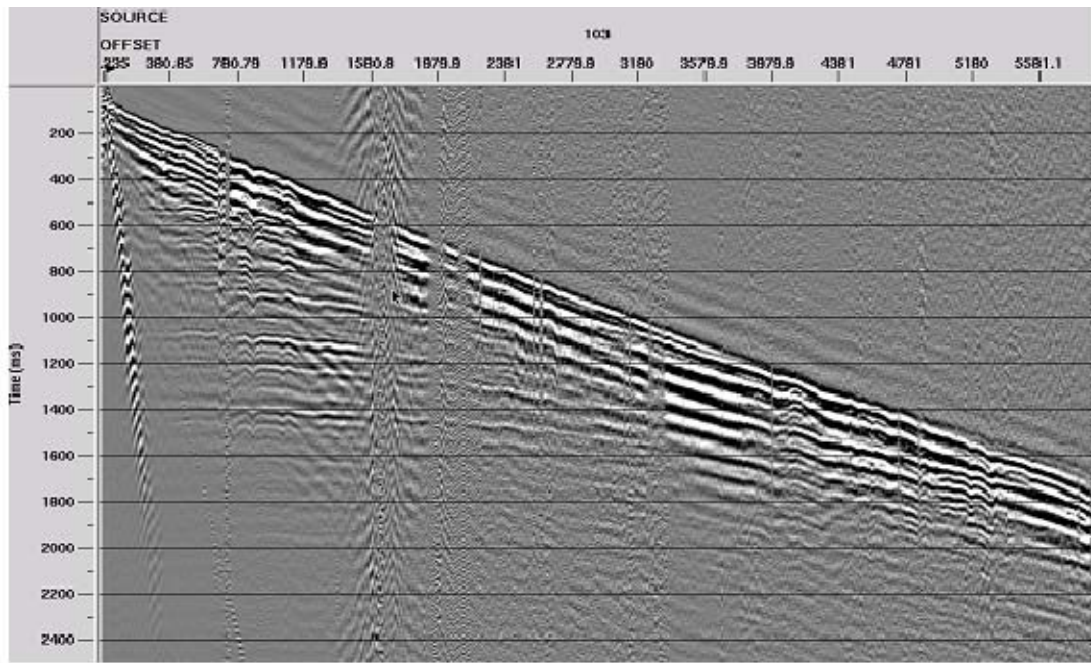
Although both of our data examples are 2D-3C lines, that is their only similarity. Our experimental, very high resolution line from the Priddis test site consisted of a 200m spread of 3C geophones planted at 1m intervals. The source positions were laterally offset from the line by 5m and extended 100m past both ends of the receiver spread, so that maximum offsets were 300m. The University of Calgary mini-vibrator was the source for the survey, and source interval was 10m. Because a concurrent test of a landstreamer (Suarez 2008) was conducted using the same source, the vibrator occupied each source position nine times (allowing the 20 m landstreamer to be moved up by one length between each pass of the vibrator down the source line). At this site, coherent source-generated noise is a considerable problem, and the shot gathers show considerable trace-to-trace variation in S/N, providing a particular challenge for deconvolution of any variety. These data would probably be rated as only poor to fair in quality. Figure 1 shows an example of an unprocessed shot gather from this line.



Priddis shot 401, bandpass 8-12-150-200 Hz

FIG. 1. Typical shot gather from Priddis experiment, before filtering.

The Spring Coulee survey, on the other hand, a 6.5 km 2D-3C line of more conventional dimensions (10m geophone spacing), is little affected by coherent noise and exhibits much less variation from trace to trace, except for a few surface locations affected by local noise sources. The geophone spread for this line consisted of 652 3C phones, so that offsets were as large as 6520 m, or more than 20 times the maximum offset of the Priddis data set. The extremely high S/N of these data means that they would easily be rated as excellent in quality. An unprocessed shot gather from this line is shown in Figure 2.



Spring Coulee vertical component raw shot gather

FIG. 2. Typical shot gather from Spring Coulee, before filtering.

PROCESSING PROCEDURE

The success of any deconvolution algorithm is ultimately judged on the basis of how well it removes the effects of source characteristics, receiver coupling, field geometry, earth filtering, and additive noise from seismic traces, to leave the desired “earth function”, or reflectivity. Consequently, while we will exhibit individual shot gathers, we will emphasize the comparison of final stacked sections in terms of their geological interpretability. Furthermore, we compare only different formulations of the Gabor deconvolution algorithm introduced by Margrave et al (2003), rather than other deconvolution schemes commonly used in the seismic industry. The final judgment on the success of the Gabor techniques compared with others will be up to those engaged in seismic interpretation.

Over the years, we have evolved a processing strategy for applying Gabor deconvolution which is as follows:

- Filter the raw source gathers to remove as much coherent noise as possible. Radial trace filtering, in both its fan filter and dip filter modes is useful for this, since it allows the user to specifically identify and remove each linear noise system in succession, like peeling an onion.
- Apply linear moveout to approximately flatten the first arrivals of the source gathers, so that deconvolution windows are positioned similarly on all traces, regardless of offset.
- Apply whichever version of Gabor deconvolution is desired.

- Remove the linear moveout.

Source gathers prepared as above may be compared directly to examine the differences between algorithms; or they may be corrected for NMO and stacked over CDP to provide a more realistic comparison for actual interpretability. Our usual practice is to apply a post-stack pass of *Gabor2* with a long window, in single trace mode, as a post-stack spectral whitener. If linear noise survives the stack, it can be further removed using post-stack radial trace dip filtering. A pass or two of FX-decon then removes background random noise to further clean the section. While post-stack time migration can be applied, we find that data comparisons show more detailed differences if we do post-stack dip filtering and FX-decon instead. In every case we compare, all pre-stack and post-stack processing is identical, so that the only differences in the images are due to the particular pre-stack deconvolution applied.

Interpretability is a very subjective judgment; therefore, in what follows, we refrain from declaring that one image is closer to the geological “truth” than another. We will, however, comment on what we see as significant visible differences and leave it up to the reader to express a preference.

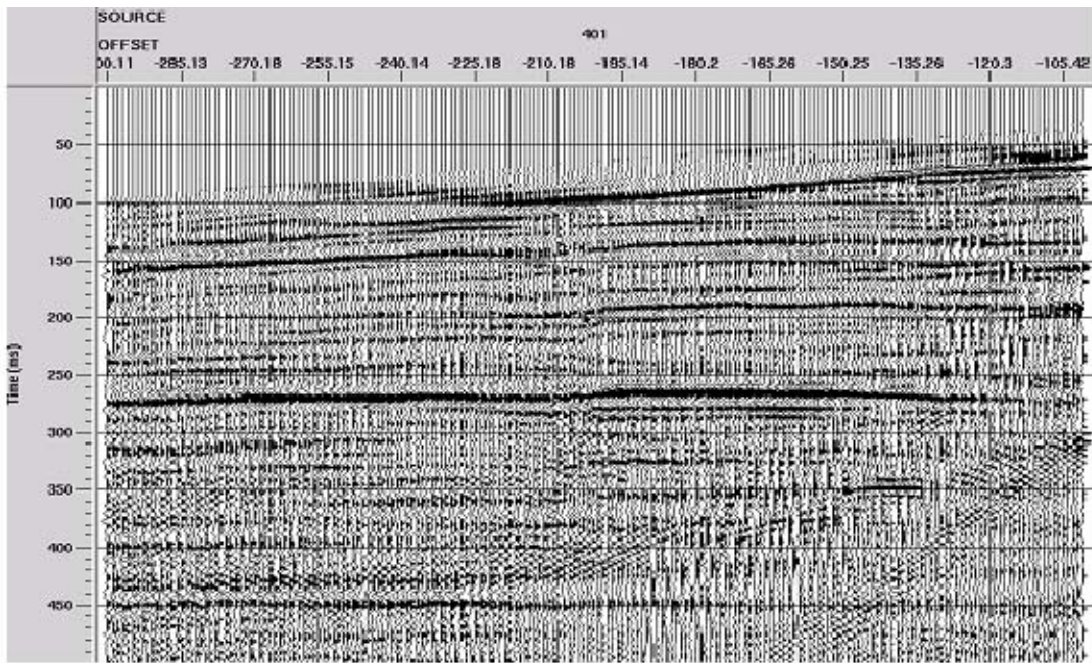
THE PRIDDIS EXPERIMENT

In 2006, CREWES and University staff conducted a field experiment near Longview, Alberta whose objective was to explore the benefits of acquiring seismic data using very finely spaced single geophones instead of the more coarsely spaced series-wired ‘groups’ of phones typically used for seismic surveys (Henley et al, 2006). In that survey, we planted a 1 km 2D seismic line with single vertical component geophones spaced 2.5 m apart, and recorded each phone individually as we moved the source (our mini-vibe) through the spread from one end to the other. We subsequently processed the data in their original full resolution, then synthesized four other data sets from the original to simulate surveys performed with conventional geophone arrays spaced at 5 m, 10 m, 20 m, and 40 m. In each case, we visually analyzed shot records from the individual surveys to determine the appropriate coherent noise attenuation parameters, then applied the NMO and residual statics determined from the 2.5 m survey to each of the others, in order to eliminate any possible processing differences between the five surveys (except only the noise filtering). What we found was that we could most easily analyze and remove the various coherent noise modes on the 2.5 m survey, and that as spatial resolution decreased to 5, 10, 20, and 40 m, more and more of the modes became aliased and eventually undetectable as linear noise. The residual linear noise on the shot records in turn determined the degree of spectral whitening achievable during the deconvolution, and hence the vertical resolution. Our conclusion for this experiment was that recording single, closely spaced geophones improved both lateral and vertical resolution, and that the coherent noise suppression afforded by linear summation of geophones was always inferior to suppression by multi-channel processing of the separate geophone signals (radial trace fan filtering and dip filtering).

When examining the records from the Longview experiment, we found that even on the 2.5 m survey, some coherent noises were still partially aliased, and hence not likely to be fully attenuated by our filtering efforts. To explore resolution limits even further, we

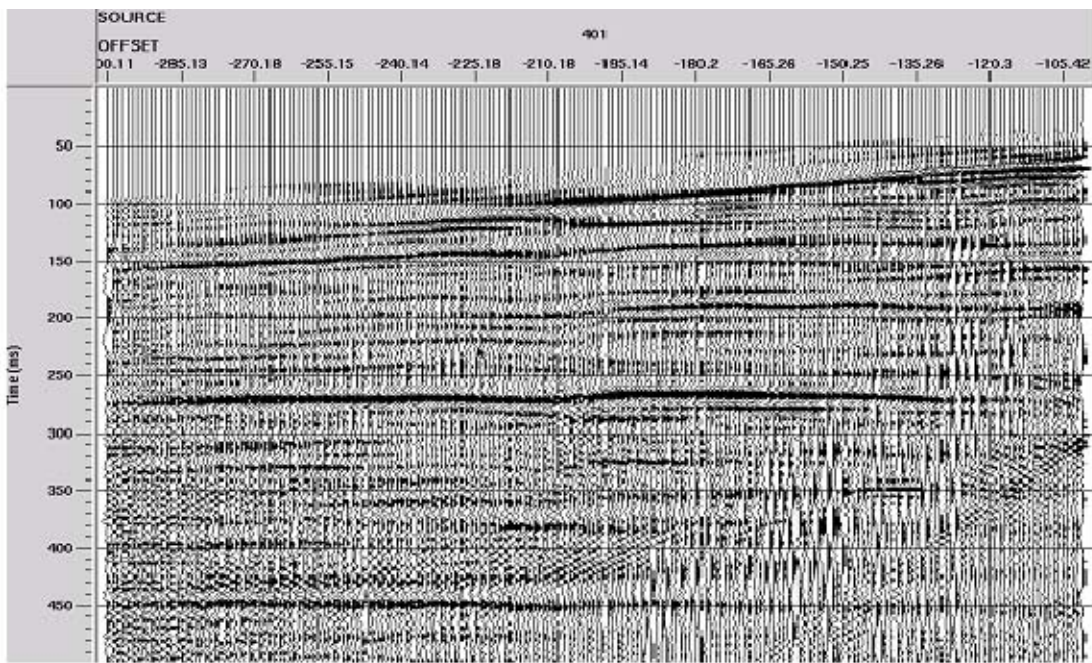
designed an experiment to be performed at our Priddis test site in which 3C geophones would be used, and in which the receiver spacing would be 1 m (Henley, et al, 2008). The geophone spread for this experiment was 200 stations long; and the shot spread, centred on the geophone spread, but offset from it by 5 m, was 400 m in length, with 10 m between shot positions. As anticipated, the individual shot records were overwhelmed by coherent noise, with no reflections visible on the raw shot records. As in the 2006 Longview experiment, however, a series of radial trace filters successfully attenuated much of the noise, so that deconvolution can be successfully applied to the data. An accompanying report chapter describes the processing and imaging of these data in more detail (Henley et al, 2008).

Figures 3, 4, 5, and 6 show the results of applying our various deconvolution schemes to the filtered shot gather whose raw form is shown in Figure 1. In Figure 3, we show the gather after application of *Gabor2* in its single trace mode, in which the Gabor deconvolution operator is derived from each individual trace and applied only to its corresponding trace. Figure 4 shows the result of *Gabor2* applied in its ensemble mode, in which the Gabor transform averaged over the entire shot gather is used to compute the single deconvolution operator which is applied to each trace in the gather. Figure 5 shows the result of 1 pass of *Gabor_sc*, in which the source, receiver, CDP, and offset-dependent components of the deconvolution operator are estimated by factoring and averaging over the line before being applied to the individual traces. Figure 6 is the deconvolution result for pass 3 of *Gabor_sc*, in which the original source, receiver, CDP, and offset-dependent estimates have been iteratively improved in a SIRT-like updating scheme before being applied to the traces. In every case, all deconvolution parameters are the same, except only the decon mode for *Gabor2* and the pass number for *Gabor_sc*.



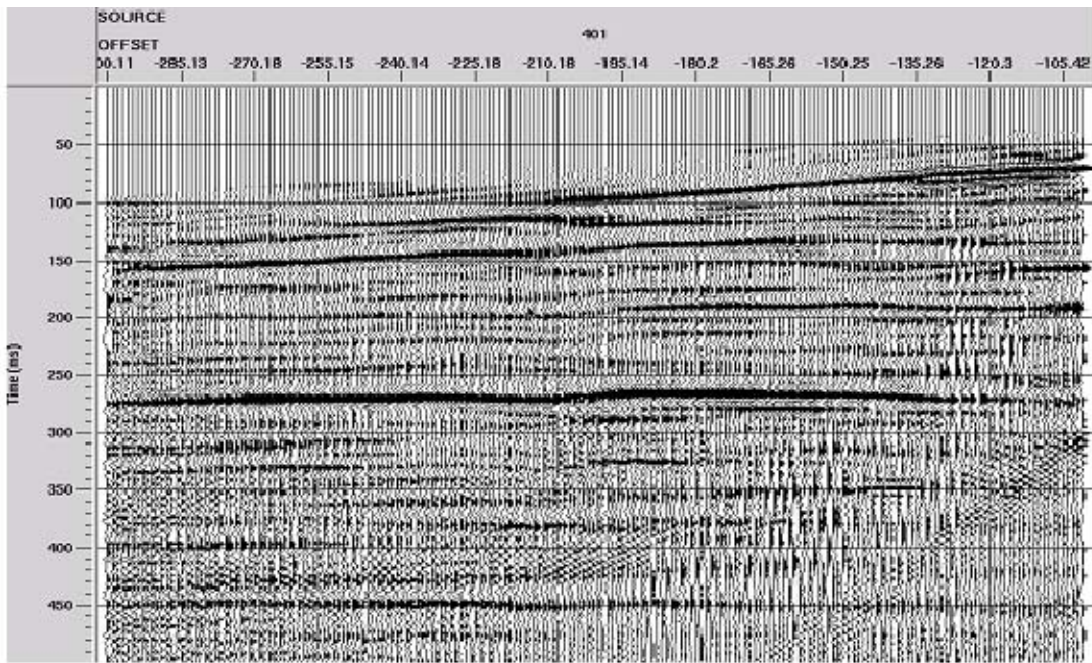
Priddis shot 401 after filtering, Gabor2 single trace mode

FIG. 3. Priddis shot gather, coherent noise attenuated, deconvolved with **Gabor2** in single trace mode.



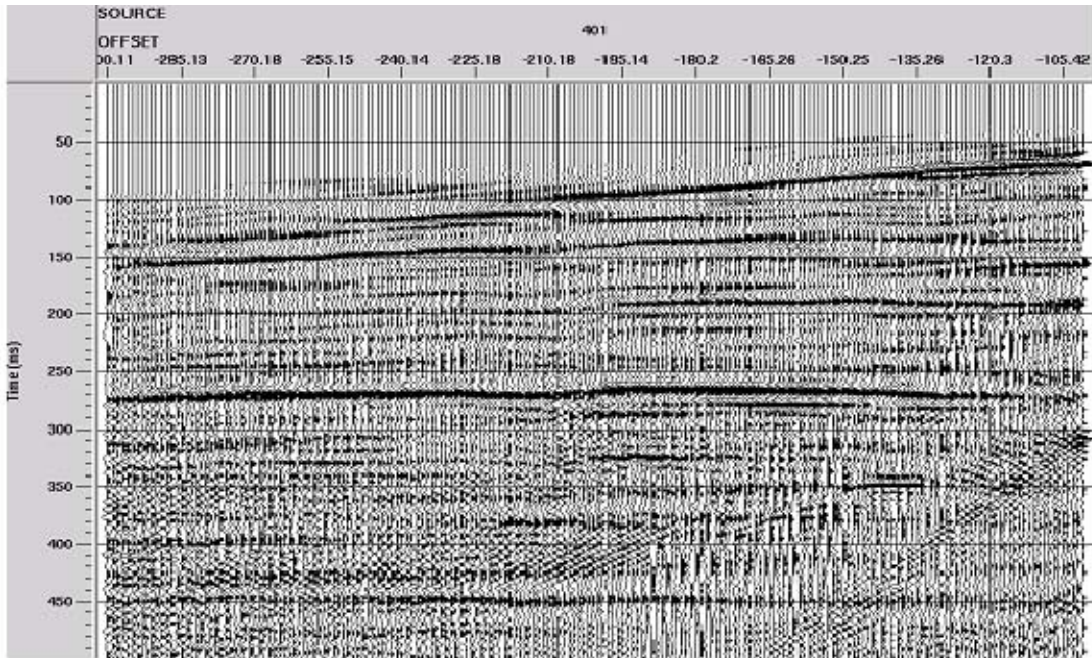
Priddis shot 401 after filtering, Gabor2 ensemble mode

FIG. 4. Priddis shot gather, coherent noise attenuated, deconvolved with **Gabor2** in ensemble mode.



Priddis shot 401 after filtering, *Gabor_sc* pass 1

FIG. 5. Priddis shot gather, coherent noise attenuated, deconvolved with *Gabor_sc* pass 1.



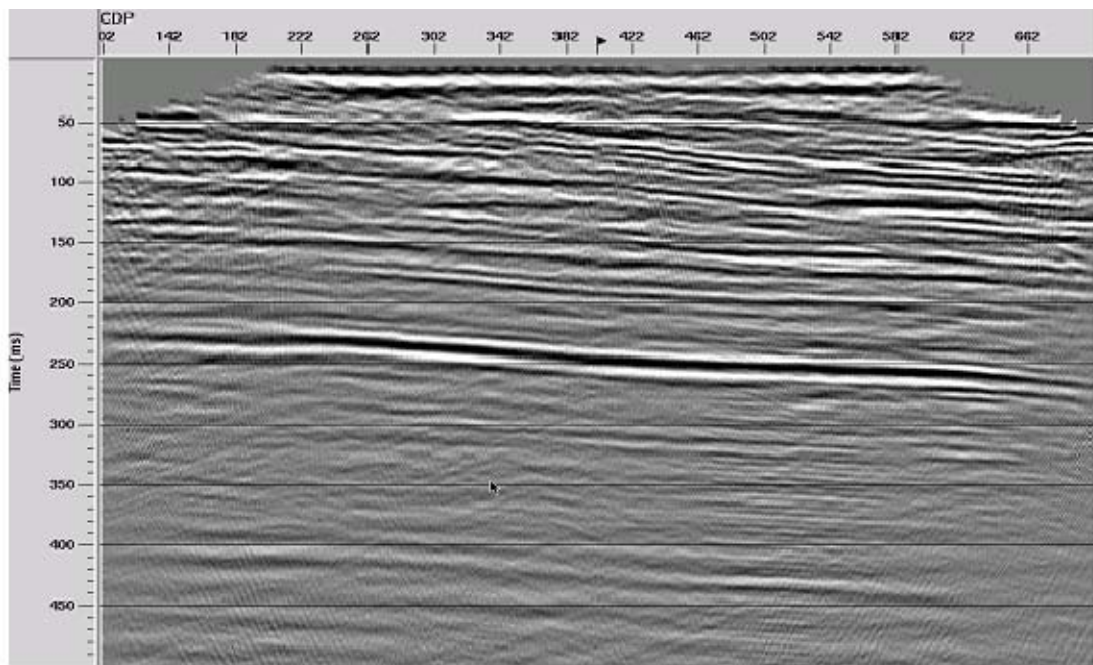
Priddis shot 401 after filtering, *Gabor_sc* pass 3

FIG. 6. Priddis shot gather, coherent noise attenuated, deconvolved with *Gabor_sc* pass 3 (iterated).

The differences we see in these deconvolved gathers are similar to those we reported last year for an earlier version of *Gabor_sc* (Henley et al, 2007). The single trace mode of

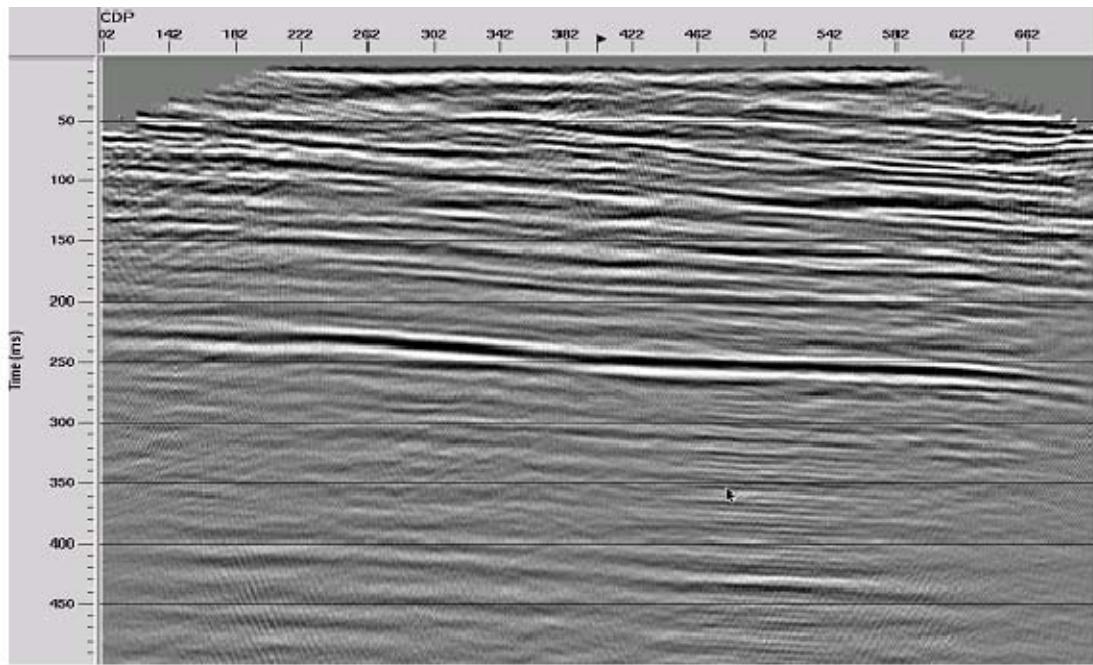
Gabor2 provides the result with the greatest bandwidth, while the phase of events from the **Gabor2** ensemble mode may possibly be more consistent over a gather. **Gabor_sc**, however, seems to combine the benefits of both; and the iteration, as seen in Figure 6, appears to improve the initial estimate shown in Figure 5. The real test of these algorithms, however, is in how their characteristics affect the interpretability of the final stacked section, after the deconvolved gathers have undergone several more stages of processing, including post-stack deconvolution in single trace mode by **Gabor2**, post-stack coherent noise attenuation, and post-stack random noise attenuation (FX decon).

To illustrate the image differences due to the choice of pre-stack deconvolution, Figures 7, 8, 9, and 10 show the final processed stack of the Priddis experiment vertical component after pre-stack deconvolution with **Gabor2** single trace mode, **Gabor2** ensemble mode, **Gabor_sc** pass 1, and **Gabor_sc** pass 3, respectively. On this scale, image differences are relatively subtle. However, the **Gabor2** single trace mode results seem to show the most shallow detail (and the most residual coherent noise), while the **Gabor_sc** results seem to have somewhat more deep resolution (from 250 ms to 500 ms).



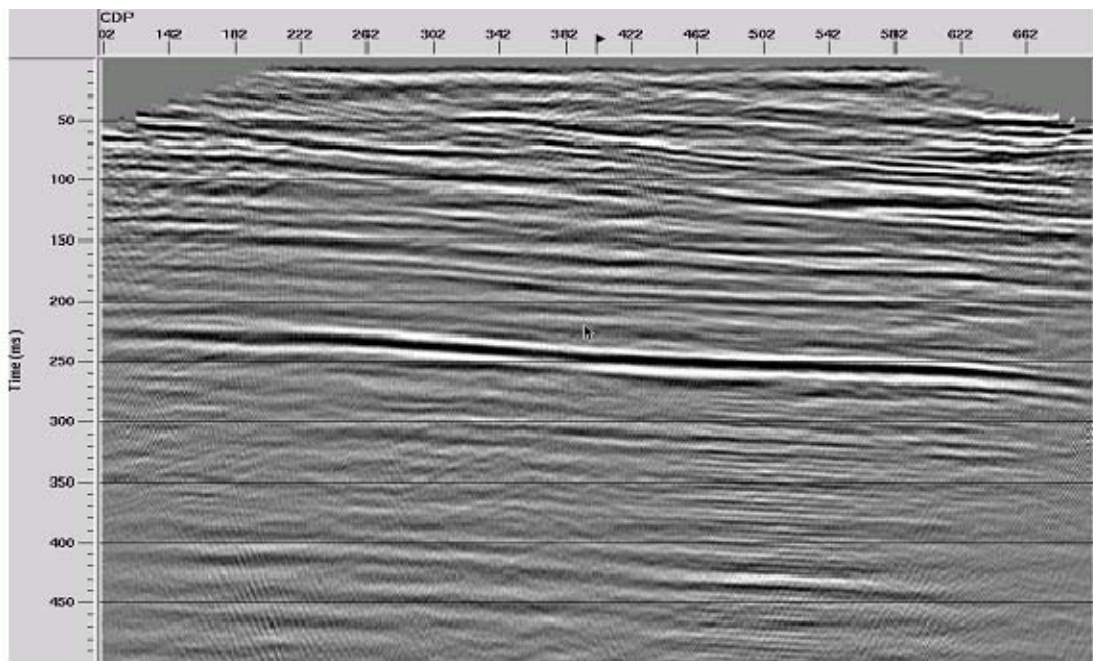
Gabor2 single trace mode, post-stack Gabor2

FIG. 7. CDP stack of shots deconvolved pre-stack with **Gabor2** single trace mode, post-stack by **Gabor2** single trace mode.



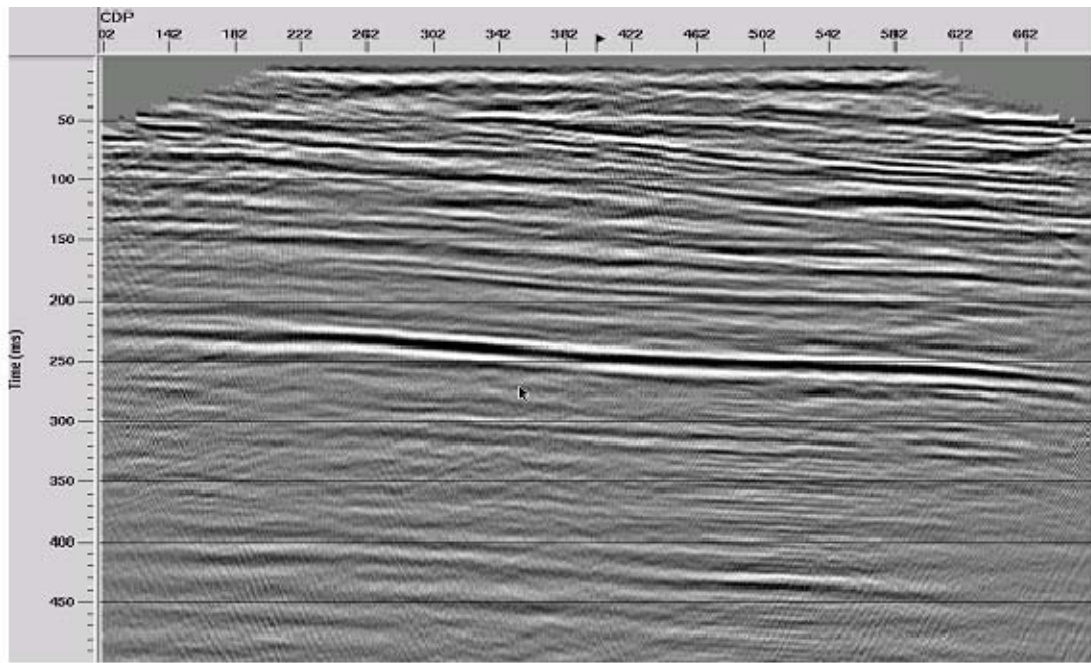
Gabor2 ensemble mode, post-stack Gabor2

FIG. 8. CDP stack of shots deconvolved pre-stack with **Gabor2** ensemble mode, post-stack with **Gabor2** single trace mode.



Gabor_sc pass1, post-stack Gabor2

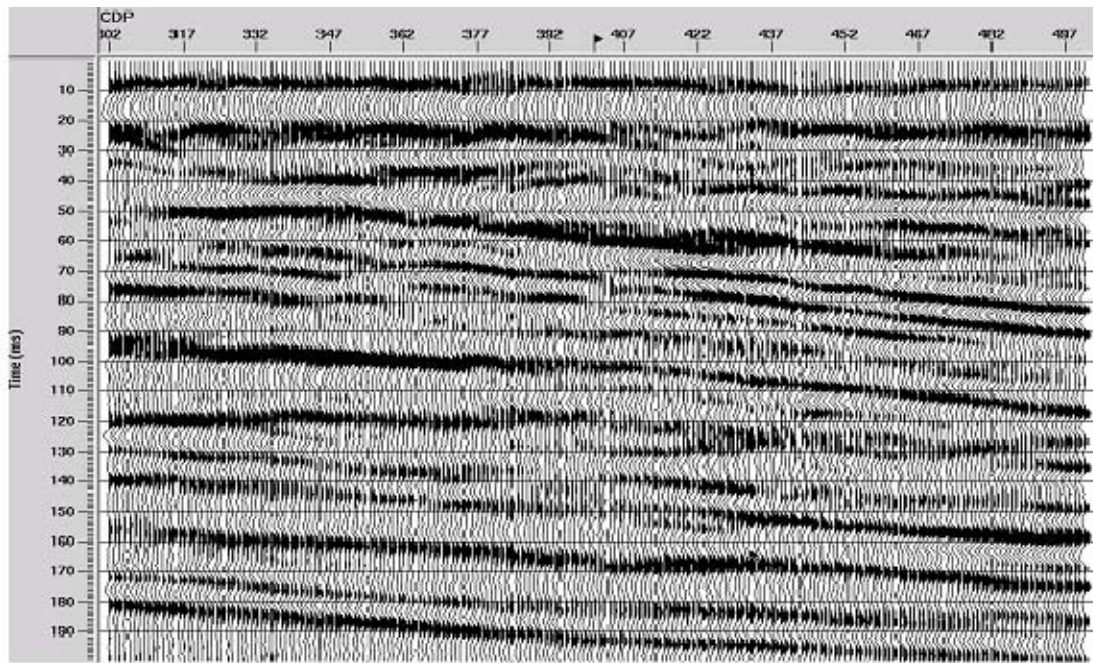
FIG. 9. CDP stack of shots deconvolved pre-stack with **Gabor_sc** pass 1, post-stack with **Gabor2** single trace mode.



Gabor_sc pass 3, post-stack Gabor2

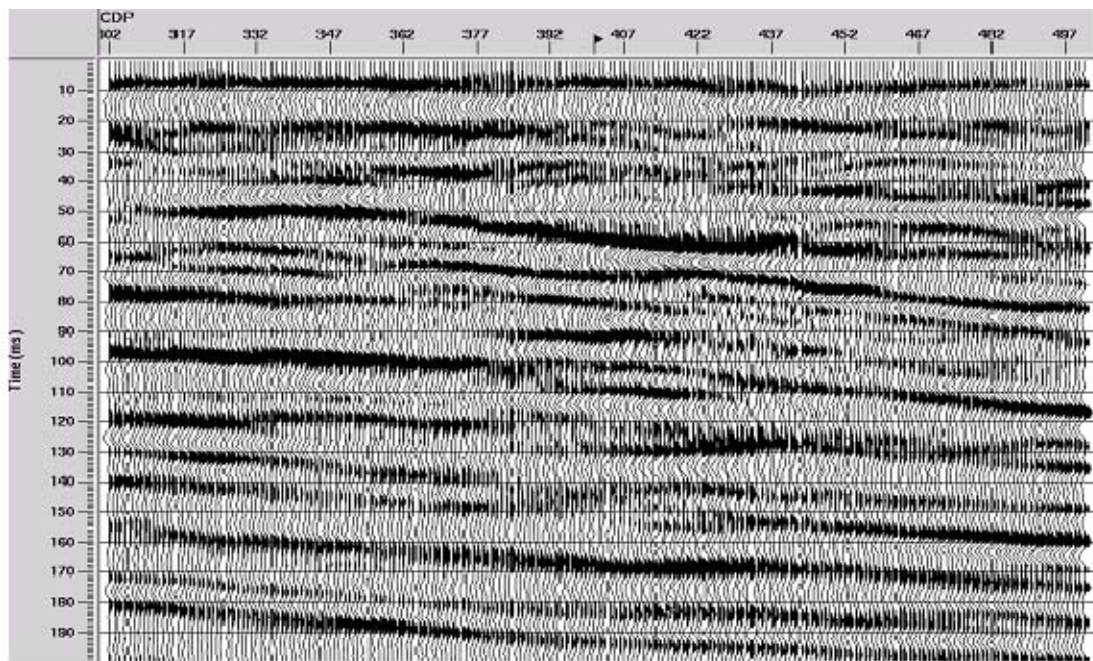
FIG. 10. CDP stack of shots deconvolved pre-stack with **Gabor_sc** pass 3, post-stack with **Gabor2** single trace mode.

For a closer look at the detail of the shallow images, we offer Figures 11, 12, 13, and 14; which show a closeup of the shallow portion of the centre of the line, where fold is highest, for **Gabor2** single trace mode, **Gabor2** ensemble mode, **Gabor_sc** pass 1, and **Gabor_sc** pass 3, respectively. Both **Gabor2** single trace mode and **Gabor_sc** pass 3 (Figures 11 and 14) seem to provide a better image of what appear to be dipping layers subcropping beneath shallow layers. Which, if either, is closer to the correct geological situation is unknown, but event phase seems slightly more consistent laterally on the **Gabor_sc** results.



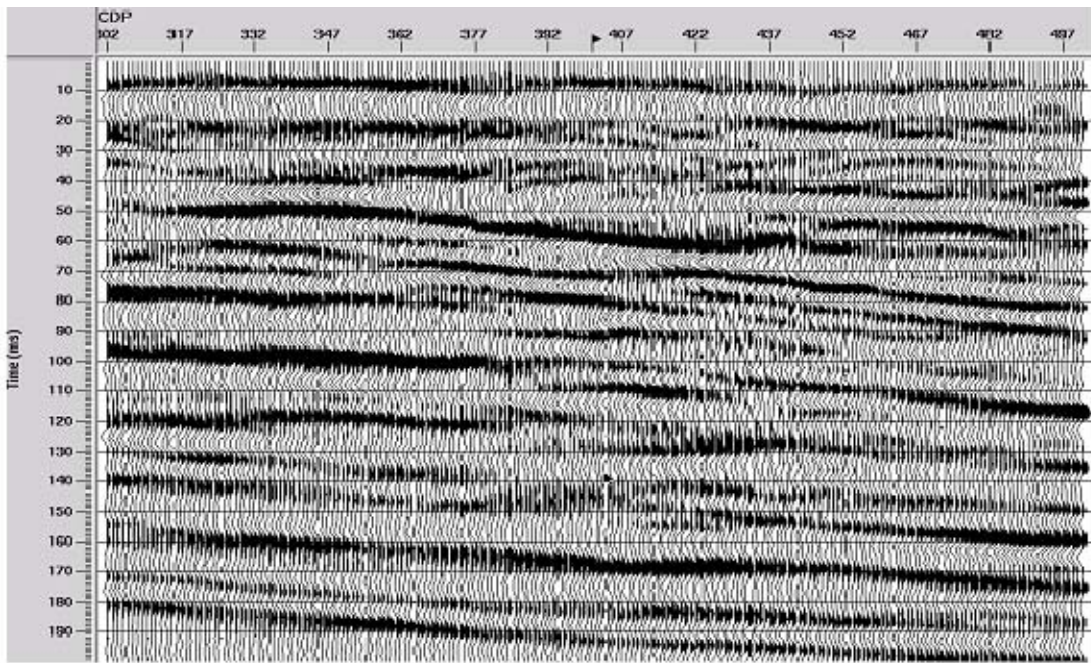
Gabor2 single trace mode, post-stack Gabor2, detail

FIG. 11. Detail of CDP stack of shots deconvolved pre-stack with **Gabor2** single trace mode, post-stack with **Gabor2** single trace mode.



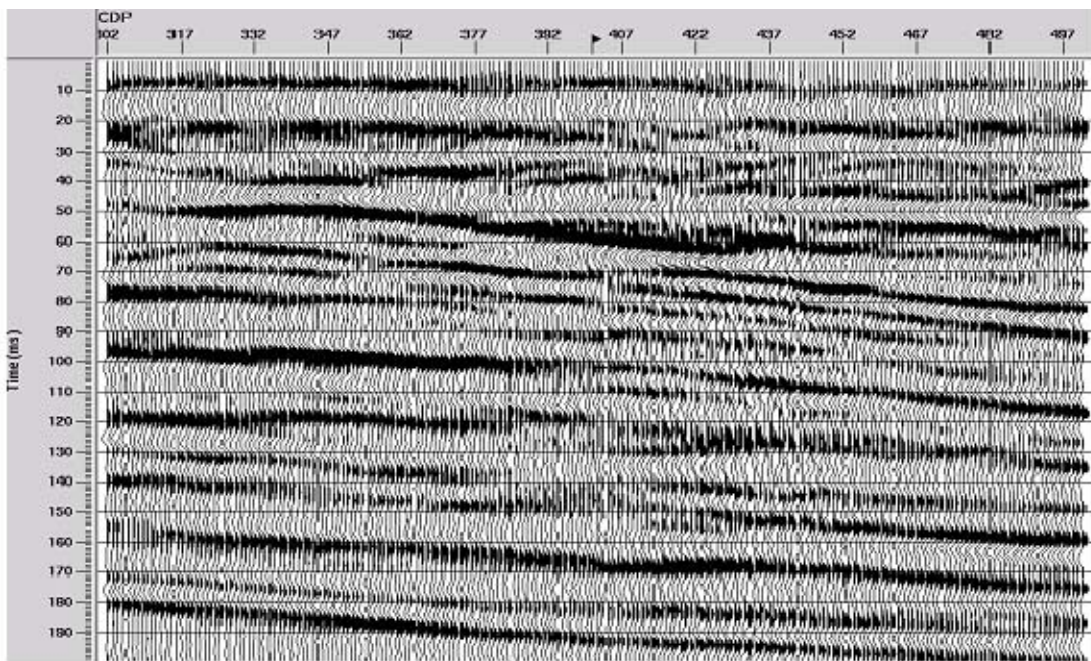
Gabor2 ensemble mode, post-stack Gabor2, detail

FIG. 12. Detail of CDP stack of shots deconvolved pre-stack with **Gabor2** ensemble mode, post-stack with **Gabor2** single trace mode.



Gabor_sc pass 1, post-stack Gabor2, detail

FIG. 13. Detail of CDP stack of shots deconvolved pre-stack with *Gabor_sc* pass 1, post-stack with *Gabor2* single trace mode.

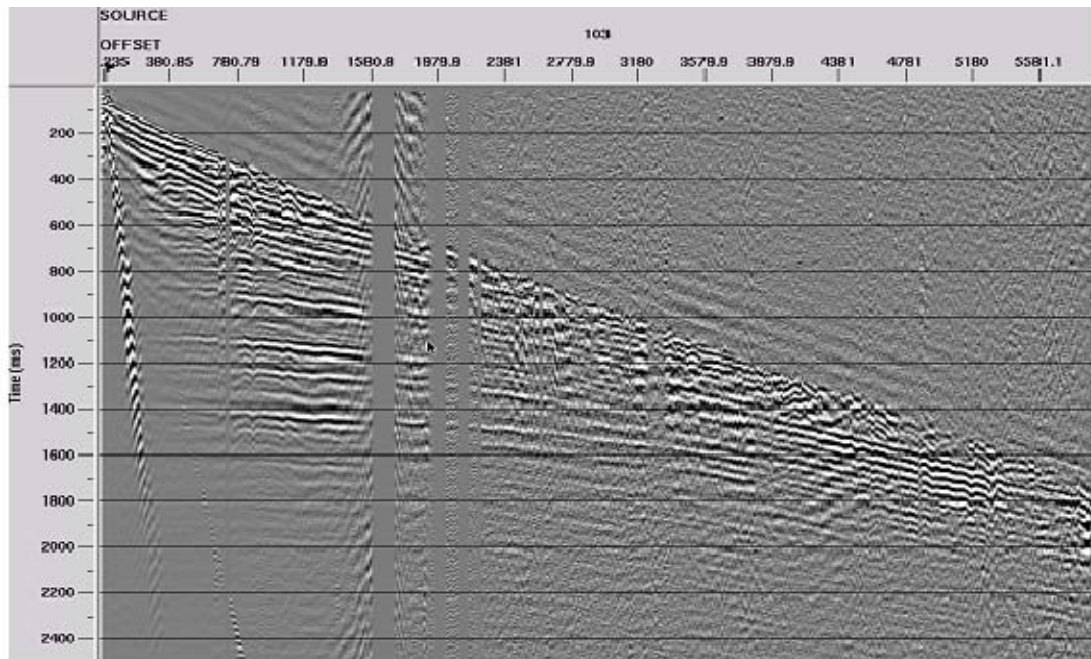


Gabor_sc pass 3, post-stack Gabor2, detail

FIG. 14. Detail of CDP stack of shots deconvolved pre-stack with *Gabor_sc* pass 3, post-stack with *Gabor2* single trace mode.

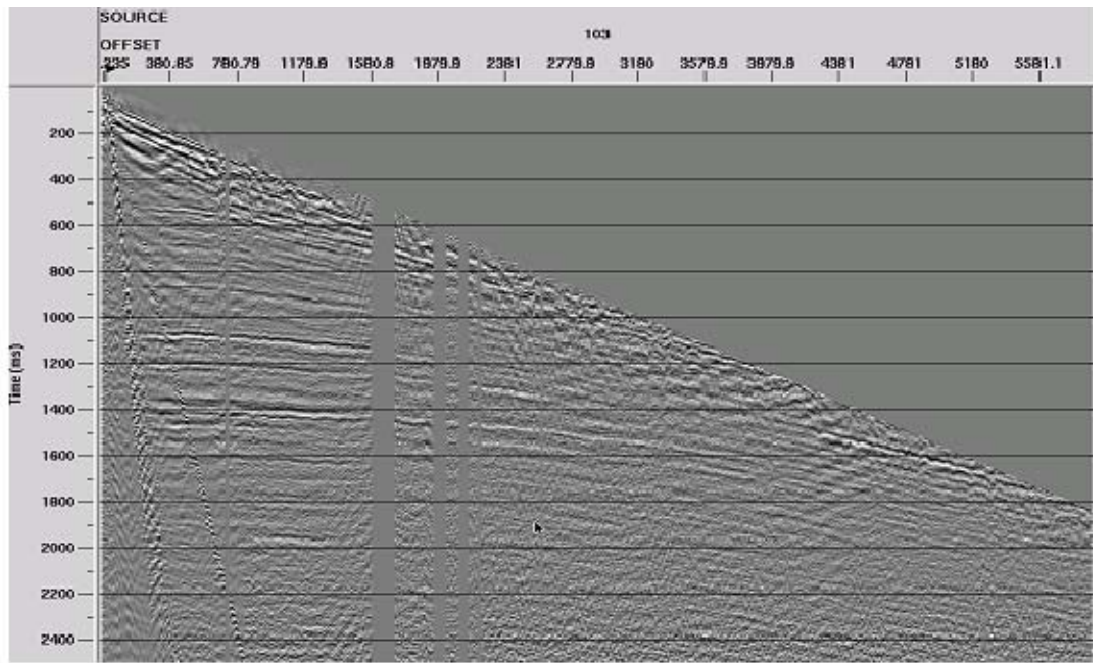
SPRING COULEE

Early in 2008, CREWES had the opportunity to participate in a 2D-3C seismic survey at Spring Coulee, south of Lethbridge, Alberta, on some land to which the University of Calgary has mineral rights. The survey was to be a direct comparison not only of geophone types (conventional vs accelerometers), but of sources as well (conventional vibrator vs mini-vibe). The data proved to be of exceptionally high quality (see Figure 1), in contrast to that in the Priddis high resolution survey. In addition, there was a significant gap in source coverage on the line. Thus it provides rather different challenges for deconvolution algorithms than the very noisy Priddis data. As Figure 1 shows, although there is coherent noise on the shot records, reflections are easily visible, regardless, and pre-stack attenuation of coherent noise would not be absolutely necessary on these data. We chose to apply one pass of radial trace fan filtering, nevertheless, and the result can be seen in Figure 15. The direct arrivals and their repeats have been largely removed from the example gather. As before, we compare this gather after application of *Gabor2* single trace mode, *Gabor2* ensemble mode, *Gabor_sc* pass 1, and *Gabor_sc* pass 3 in figures 16, 17, 18, and 19, respectively. As in all other cases examined, single trace mode *Gabor2* produces the greatest bandwidth, as well as the greatest attenuation of residual coherent noise, followed closely by *Gabor_sc* pass 3. As before, it is difficult to draw any real conclusions from shot gathers alone. Hence, we proceed to the comparison of stacked sections, which have been post-stack deconvolved with *Gabor2* single trace mode, as well as migrated with a post-stack Kirchhoff algorithm. We examine three closeup portions of the resulting stacks in order to compare the pre-stack deconvolution response to three different image features.



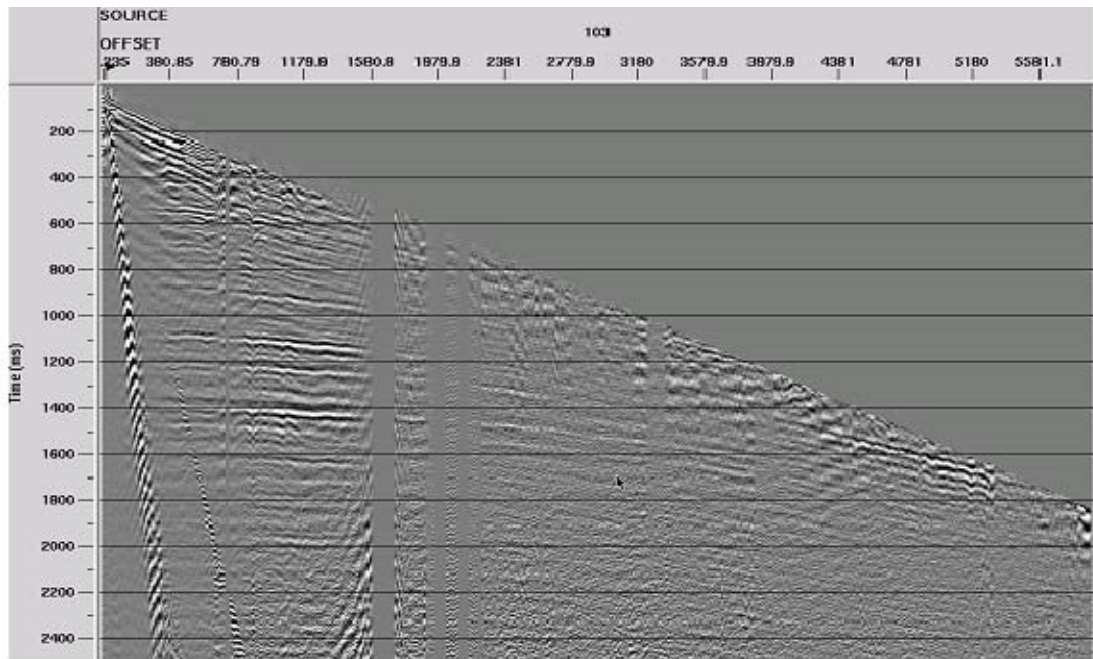
Spring Coulee vertical component shot gather after coherent noise filtering

FIG. 15. Spring Coulee vertical component shot gather after noise attenuation



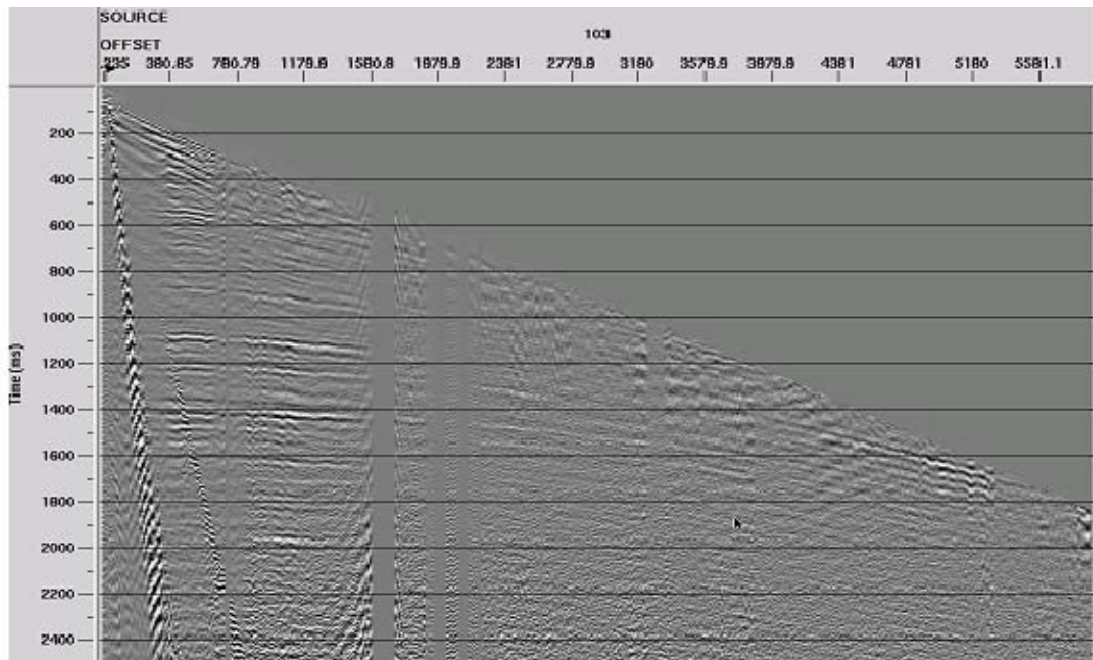
Spring Coulee vertical component shot gather after filtering, Gabor2 single trace mode

FIG. 16. Shot gather after coherent noise attenuation, deconvolved with **Gabor2** single trace mode.



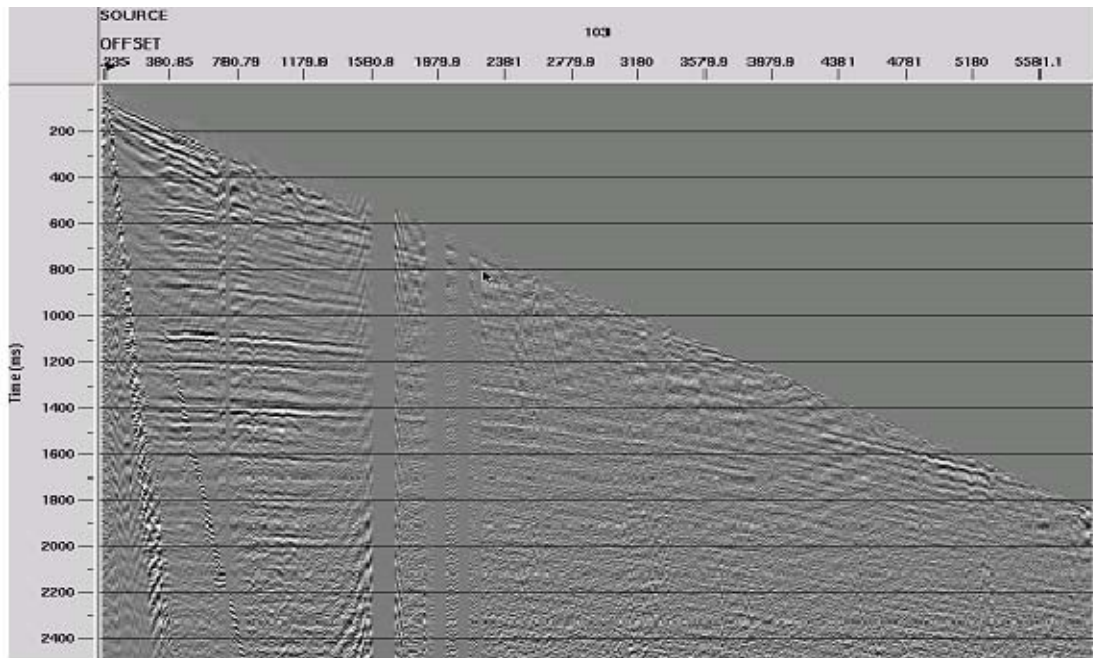
Spring Coulee vertical component shot gather after filtering, Gabor2 ensemble mode

FIG. 17. Shot gather after coherent noise attenuation, deconvolved with **Gabor2** ensemble mode.



Spring Coulee vertical component shot gather after filtering, *Gabor_sc* pass 1

FIG. 18. Shot gather after coherent noise attenuation, deconvolved with *Gabor_sc* pass 1

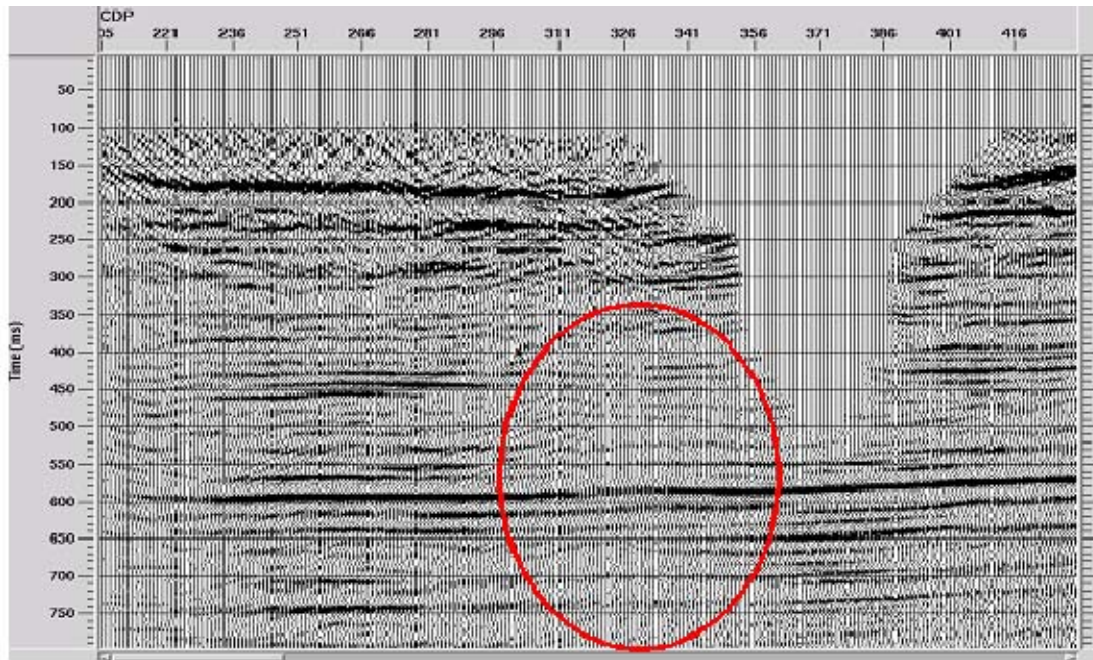


Spring Coulee vertical component shot gather after filtering, *Gabor_sc* pass 3

FIG. 19. Shot gather after coherent noise attenuation, deconvolved with *Gabor_sc* pass 3.

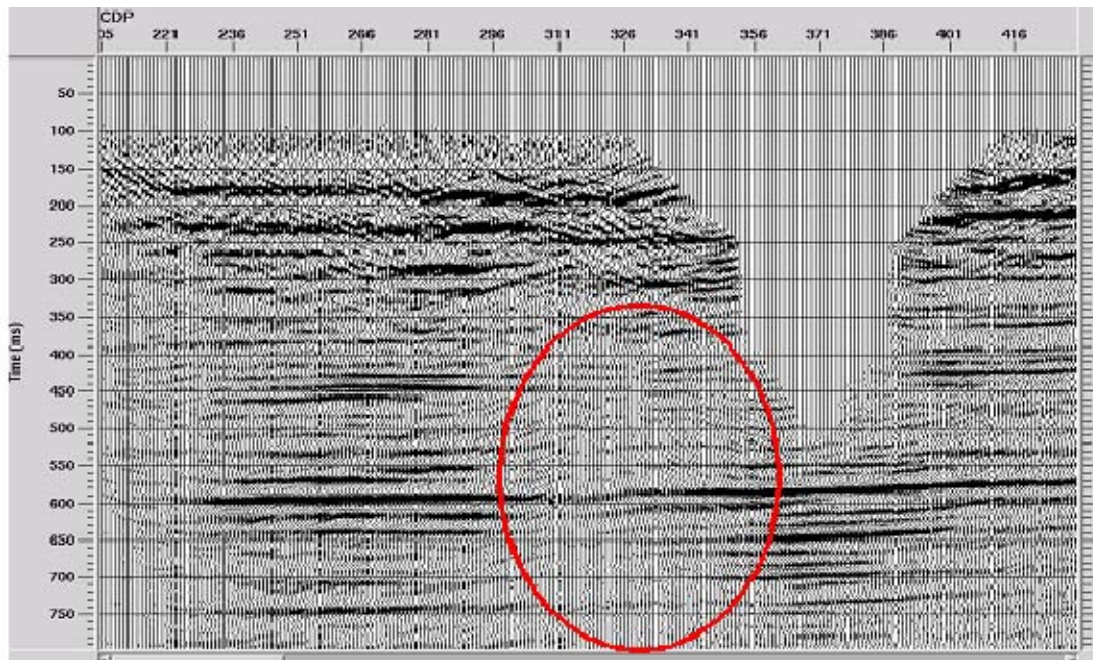
Figure 20 shows a shallow portion of the Spring Coulee line where there is a gap in source coverage due to surface features. The pre-stack deconvolution applied in this case is *Gabor2* single trace mode. Figures 21, 22, and 23 show the same section, but with

Gabor2 ensemble mode, *Gabor_sc* pass 1, and *Gabor_sc* pass 3 used respectively as the pre-stack deconvolution operations. Since one of the known weaknesses of some deconvolution approaches is the loss of amplitude and coherence of some events in the vicinity of gaps in surface coverage, we examine these figures for differences in this regard. The red ellipse highlights two events whose response clearly differs between the four figures. The best continuity of amplitude and character for both events clearly occurs with the use of either *Gabor2* single trace mode or *Gabor_sc* pass 3, with the latter giving slightly better results for the deeper, stronger reflection.



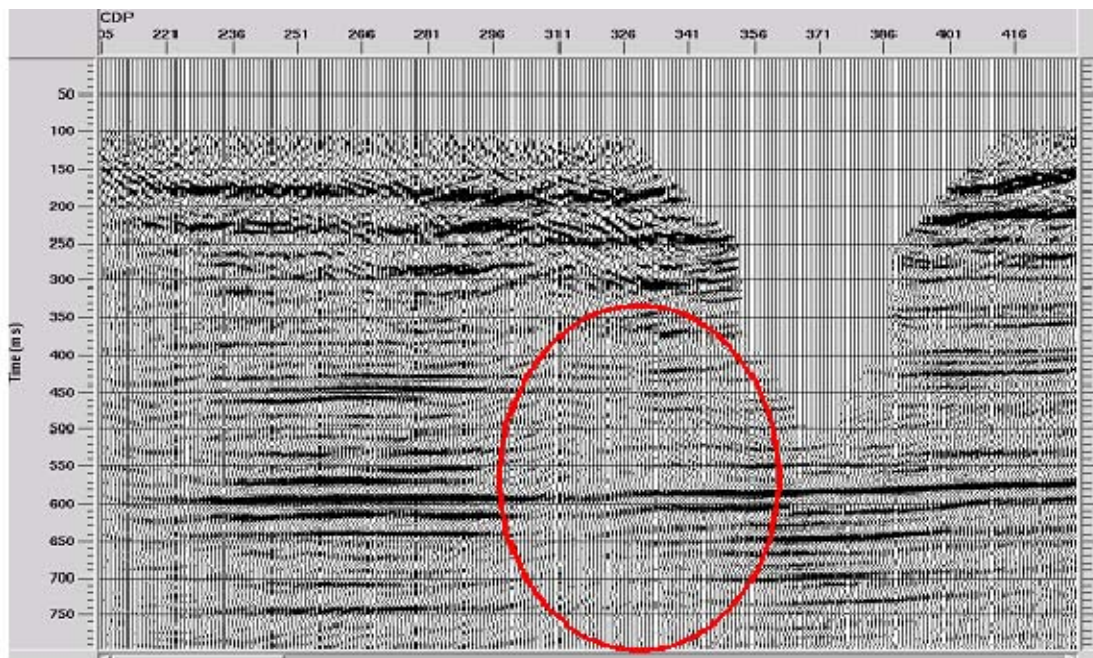
Gabor2 single trace mode, post-stack Kirchhoff, Gabor2

FIG. 20. CDP stack of shots deconvolved pre-stack with *Gabor2* single trace mode, post-stack with *Gabor2* single trace mode.



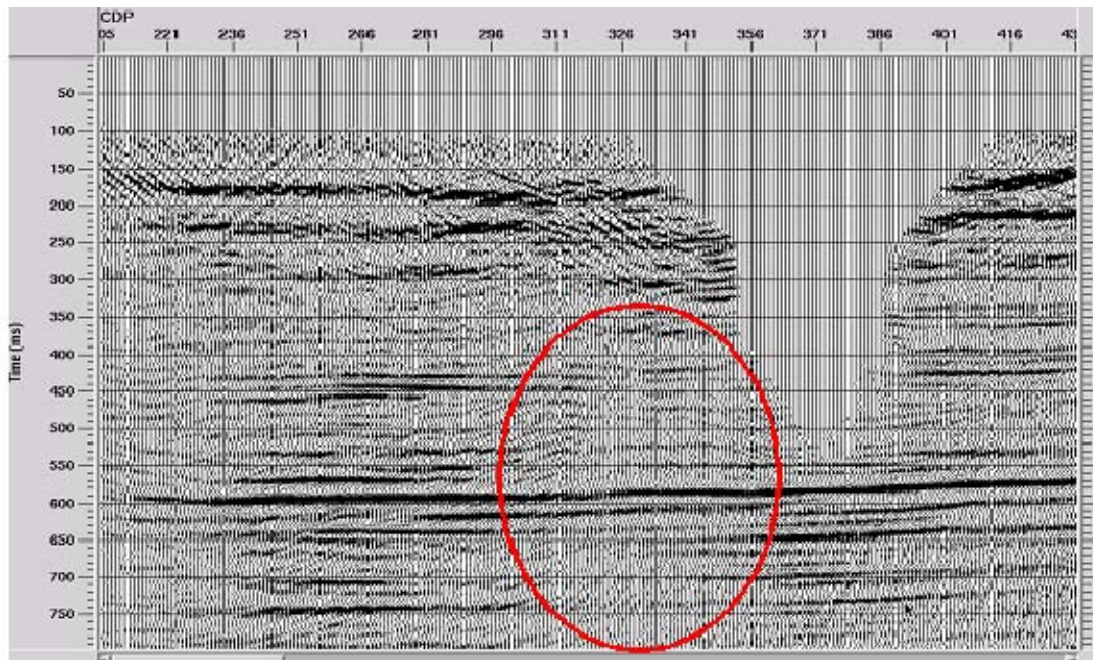
Gabor2 ensemble mode, post-stack Kirchhoff, Gabor2

FIG. 21. CDP stack of shots deconvolved pre-stack with **Gabor2** ensemble mode, post-stack with **Gabor2** single trace mode.



Gabor_sc pass 1, post-stack Kirchhoff, Gabor2

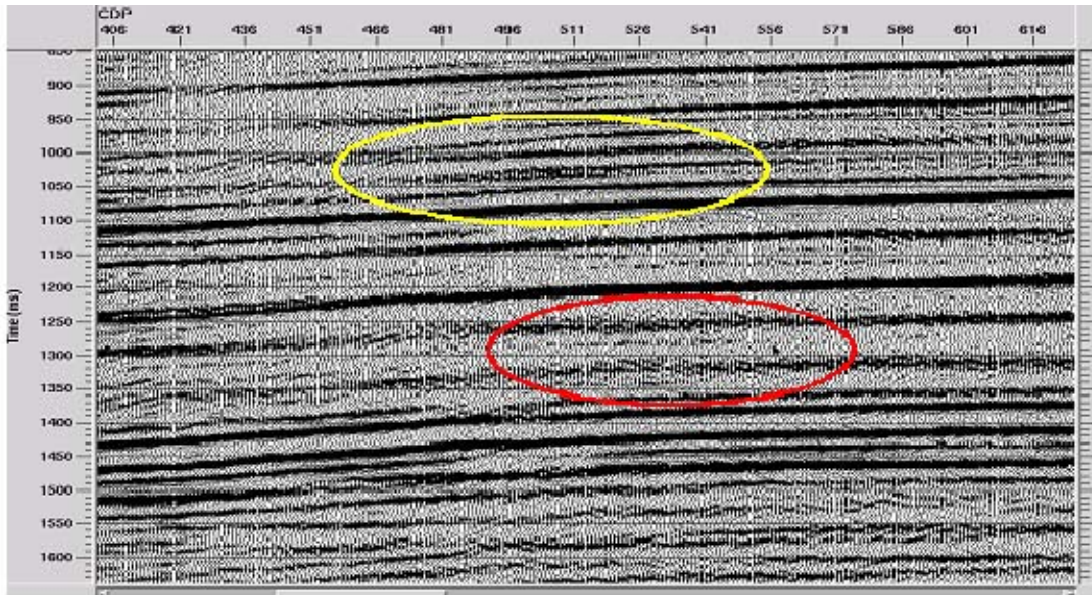
FIG. 22. CDP stack of shots deconvolved pre-stack with **Gabor_sc** pass 1, post-stack with **Gabor2** single trace mode.



Gabor_sc pass 3, post-stack Kirchhoff, Gabor2

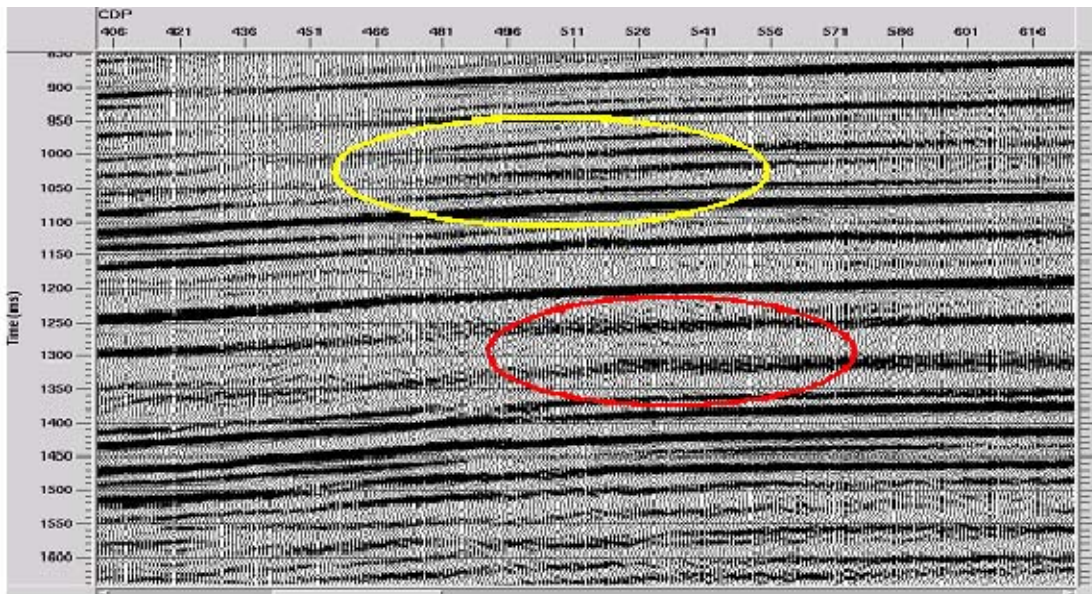
FIG. 23. CDP stack of shots deconvolved pre-stack with **Gabor_sc** pass 3, post-stack with **Gabor2** single trace mode.

Figures 24, 25, 26, and 27 display a structural feature on the Spring Coulee line, and show its internal detail at several levels (highlighted by yellow and red ellipses). The yellow ellipse outlines a pair of ‘wedge’ events which seem to thicken up-dip on the structure, while the red ellipse centres on a very faint ‘flat’ event at deeper levels in the structure. What the significance of these events is, if any, is left to the interpreter; but the influence of the choice of pre-stack deconvolution is clearly seen by comparing these four figures.



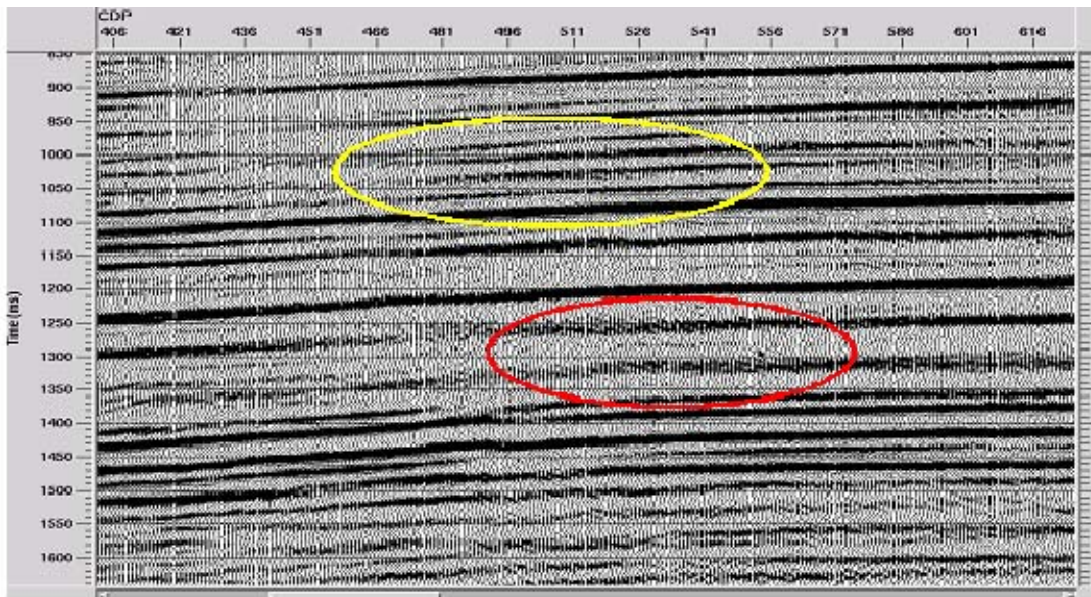
Gabor2 single trace mode, post-stack Kirchhoff, Gabor2

FIG. 24. CDP stack of shots deconvolved pre-stack with **Gabor2** single trace mode, post-stack with **Gabor2** single trace mode.



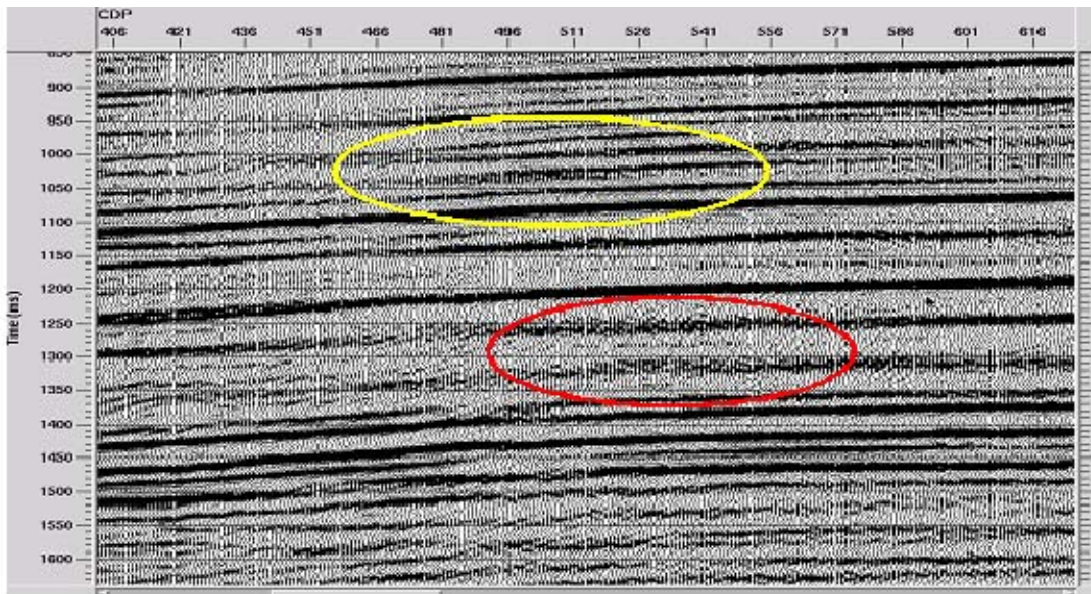
Gabor2 ensemble mode, post-stack Kirchhoff, Gabor2

FIG. 25. CDP stack of shots deconvolved pre-stack with **Gabor2** ensemble mode, post-stack with **Gabor2** single trace mode.



Gabor_sc pass 1, post-stack Kirchhoff, Gabor2

FIG. 26. CDP stack of shots deconvolved pre-stack with **Gabor_sc** pass 1, post-stack with **Gabor2** single trace mode.

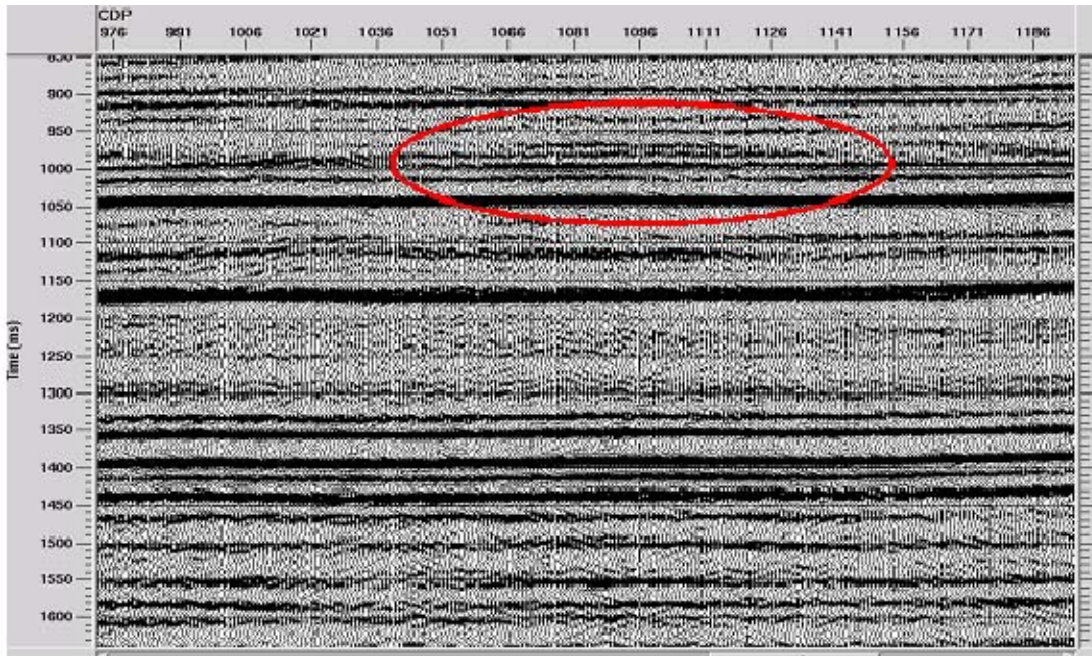


Gabor_sc pass 3, post-stack Kirchhoff, Gabor2

FIG. 27. CDP stack of shots deconvolved pre-stack with **Gabor_sc** pass 3, post-stack with **Gabor2** single trace mode.

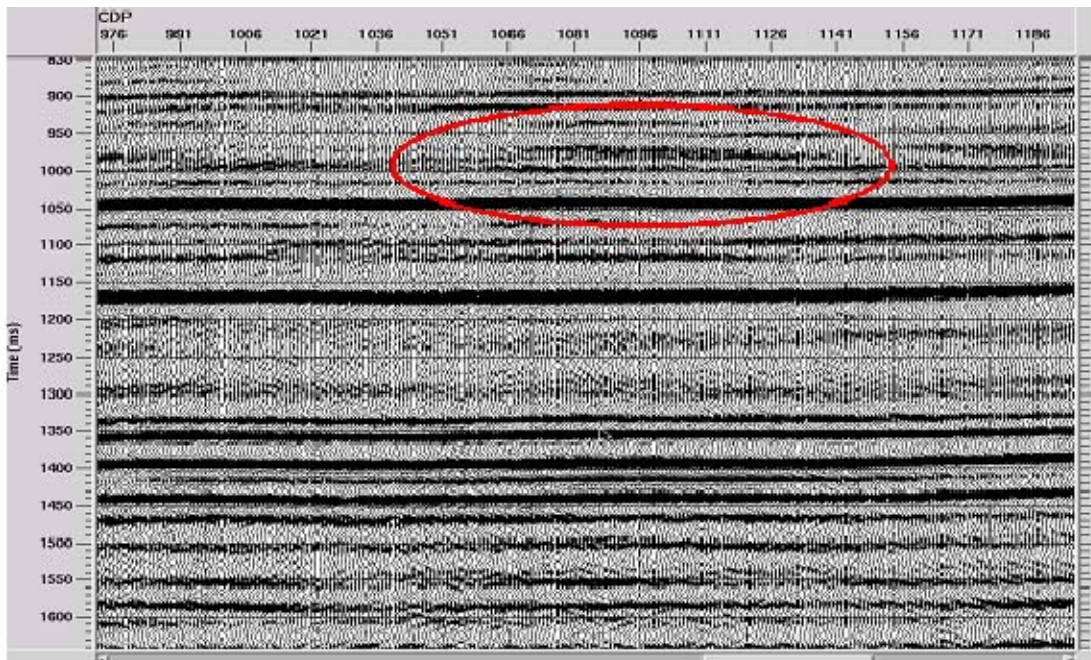
The final comparison of pre-stack deconvolution algorithms is shown in Figures 28, 29, 30, and 31, where the feature of interest (red ellipse) is an event which seems to strengthen into a doublet within the ellipse. Again, this is an exercise in judgment for an interpreter; but the highest resolution is shown for both the **Gabor2** single trace mode and the **Gabor_sc** pass 3 results. The latter seems to show somewhat better phase stability for

a variety of events, but once again, it is the interpreter who will need to judge the significance.



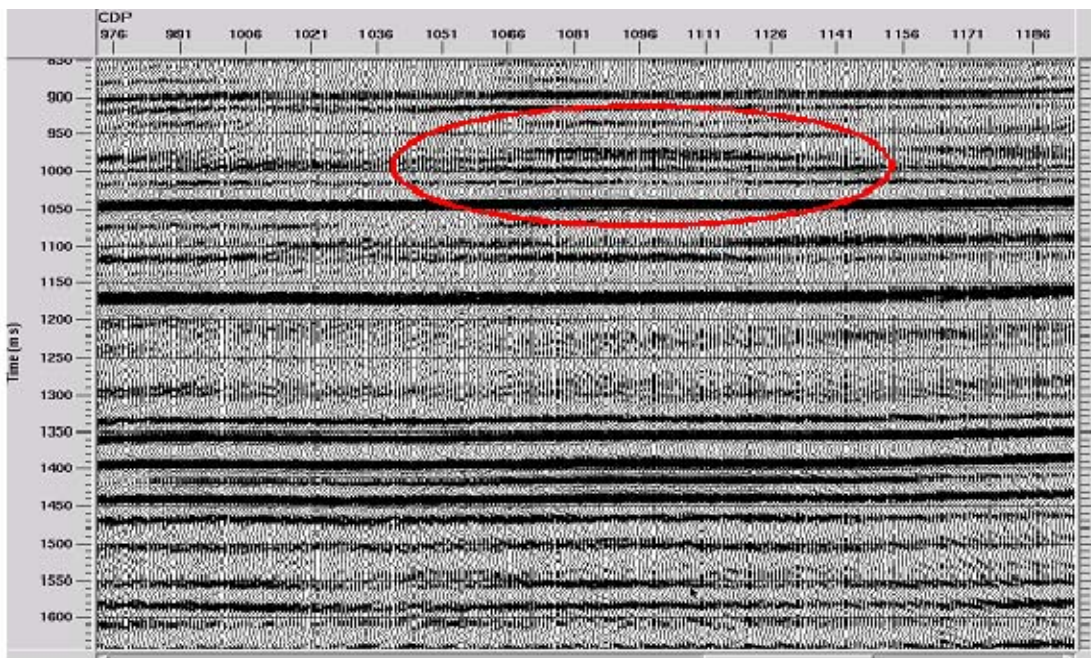
Gabor2 single trace mode, post-stack Kirchhoff, Gabor2

FIG. 28. CDP stack of shots deconvolved pre-stack with **Gabor2** single trace mode, post-stack with **Gabor2** single trace mode.



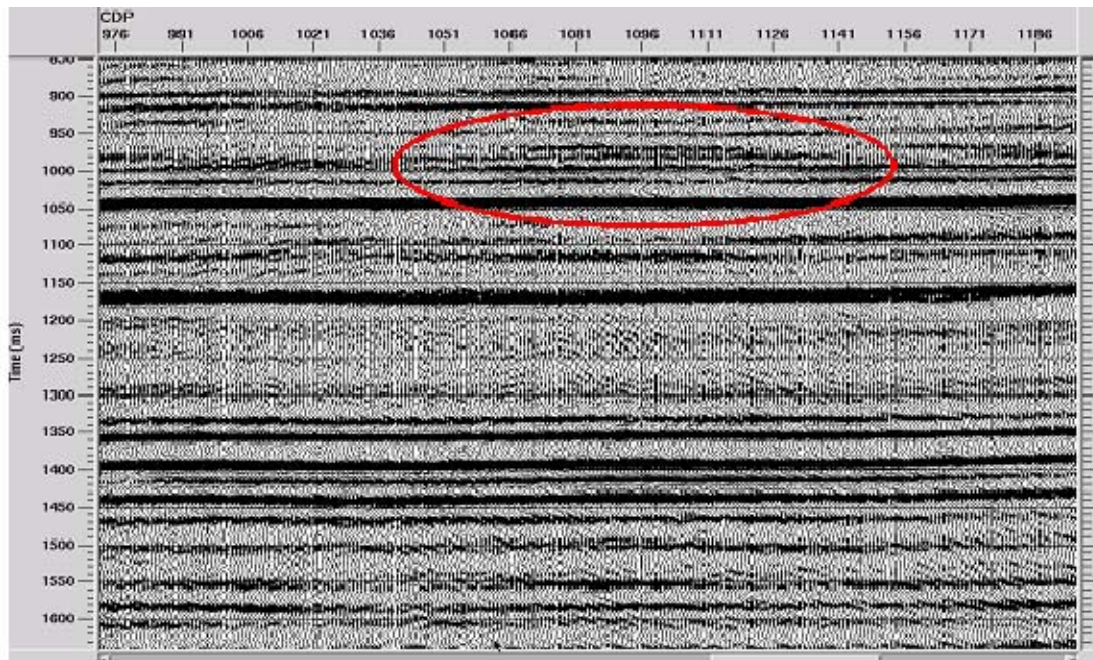
Gabor2 ensemble mode, post-stack Kirchhoff, Gabor2

FIG. 29. CDP stack of shots deconvolved pre-stack with **Gabor2** ensemble mode, post-stack with **Gabor2** single trace mode.



Gabor_sc pass 1, post-stack Kirchhoff, Gabor2

FIG. 30. CDP stack of shots deconvolved pre-stack with **Gabor_sc** pass 1, post-stack with **Gabor2** single trace mode.



Gabor_sc pass 3, post-stack Kirchhoff, Gabor2

FIG. 31. CDP stack of shots deconvolved pre-stack with **Gabor_sc** pass 3, post-stack with **Gabor2** single trace mode.

CONCLUSIONS

We have illustrated the use of four-component, iterative Gabor deconvolution, **Gabor_sc**, on two quite different data sets, with the goal of showing the very subtle differences between the results of this algorithm and the results of **Gabor2**, an earlier program which allows two modes of application. At our current level of experience with the algorithms, we might offer the following guidelines for selecting which of the algorithms to use for a given data set:

- For data sets with high S/N on all traces of every shot gather, with no large gaps in shot surface coverage, and small variability in the quality (overall S/N) of shots, **Gabor2** in the single trace mode is probably the best choice and will yield the broadest band result.
- For data sets with S/N varying considerably for traces within shot gathers, but no great variability in the quality of shots, and no large gaps in coverage, **Gabor2** in the ensemble mode is a likely choice.
- When S/N varies considerably on the traces within shot gathers, shot quality varies greatly from shot to shot, and/or large gaps in shot coverage exist, **Gabor_sc** is probably the best choice.
- Although each iteration of **Gabor_sc** requires an extra pass through the entire data set (the first output results require two passes), the extra refinement

offered by the iteration can be worthwhile, particularly if the raw data variability is considerable.

We feel it is the role of the interpreter to determine which algorithm seems to yield the results most definitive for a particular exploration objective, and the role of the data processor to understand the characteristics of each individual data set and to suggest the algorithm most suited to each set.

ACKNOWLEDGEMENTS

The authors wish to acknowledge the influence of Carlos Montana and his surface-consistent Gabor algorithm on the design of the *Gabor_sc* algorithm. We also thank CREWES sponsors for their ongoing support and CREWES staff, particularly Kevin Hall and Han-Xing Lu for assistance with data set preparation.

REFERENCES

- Henley, D.C., Margrave, G.F., and Montana, Carlos, 2007, Gabor deconvolution: surface and subsurface consistent: CREWES 2007 Research Report, **19**.
- Henley, D.C., Bertram, Malcolm, Hall, Kevin, Bland, Henry, Gallant, Eric, and Margrave, G.F., 2006, The power of high effort seismic acquisition: the Longview experiment: CREWES 2006 Research Report, **18**.
- Henley, D.C., Hall, Kevin, Bertram, Malcolm, and Gallant, Eric, 2008, Pushing the resolution limits: the Priddis 2D 3C survey: CREWES 2008 Research Report, **20**.
- Margrave, G.F., and Lamoureux, M.P., 2001, Gabor deconvolution: CREWES 2001 research report, **13**.
- Margrave, G.F., Lamoureux, M.P., Grossman, J.P., and Iliescu, V., 2002, Gabor deconvolution of seismic data for source waveform and Q correction: 72nd Ann. Internat. Mtg. Soc. Expl. Geophys., Expanded abstracts, 2190-2193.
- Margrave, G.F., and Lamoureux, M.P., 2002, Gabor deconvolution: 2002 CSEG Annual Convention, Expanded abstracts.
- Margrave, G.F., Linping Dong, Grossman, J.P., Henley, D.C., and Lamoureux, M.P., 2003, Gabor deconvolution: extending Wiener's method to nonstationarity: CREWES 2003 research report, **15**.
- Margrave, G. F., Gibson, P. C., Grossman, J. P., Henley, D. C., Iliescu, V., and Lamoureux, M. P., 2004, The Gabor Transform, pseudodifferential operators, and seismic deconvolution, Integrated Computer-Aided Engineering, 9, 1-13.
- Montana, C., Margrave, G.F., and Henley, D.C., 2006, Surface consistent Gabor deconvolution: CREWES 2006 research report, **18**.
- Perz, M., Mewhort, L., Margrave, G.F., and Ross, L., 2005, Gabor deconvolution: real and synthetic data experiences: 2005 CSEG Annual Convention, Expanded abstracts.
- Suarez, Gabriela, 2008, Side-by-side comparison of 3C land streamer versus planted geophone data at the Priddis test site: CREWES 2008 Research Report, **20**.